CORE
Metadata, citation and similar papers at core.ac.uk
Provided by epublications@Marquette

Marquette University
e-Publications@Marquette

School of Dentistry Faculty Research and Publications

Dentistry, School of

1-1-2017

Development of 3D PCL microsphere/TiO_2 nanotube composite scaffolds for bone tissue engineering

Kimia Khoshroo
Marquette University

Tahereh S. Jafarzadeh Kashi
Tehran University of Medical Sciences

Fathollah Moztarzadeh
Amirkabir University of Technology-Iran

Mohammadreza Tahriri
Amirkabir University of Technology

Hossein E. Jazayeri
Marquette University

See next page for additional authors

Accepted version. *Materials Science and Engineering: C,* Vol. 70, No. 1 (January 1, 2017): 586-598.
DOI. © 2016 Elsevier B.V. Used with permission.

Authors
Kimia Khoshroo, Tahereh S. Jafarzadeh Kashi, Fathollah Moztarzadeh, Mohammadreza Tahriri, Hossein E. Jazayeri, and Lobat Tayebi

This article is available at e-Publications@Marquette: http://epublications.marquette.edu/dentistry_fac/175

***NOT THE PUBLISHED VERSION;* this is the author's final, peer-reviewed manuscript.** The published version may be accessed by following the link in the citation at the bottom of the page.

Development of 3D PCL Microsphere/TiO_2 Nanotube Composite Scaffolds for Bone Tissue Engineering

Kimia Khoshroo
Dental Biomaterials Department, School of Dentistry, Tehran University of Medical Sciences, Tehran, Iran
Marquette University School of Dentistry, Milwaukee, WI
Tahereh S. Jafarzadeh Kashi
Dental Biomaterials Department, School of Dentistry, Tehran University of Medical Sciences, Tehran, Iran
Fathollah Moztarzadeh
Biomaterials Group, Faculty of Biomedical Engineering, Amirkabir University of Technology, Tehran, Iran
Mohammadreza Tahriri[abc]
Dental Biomaterials Department, School of Dentistry, Tehran University of Medical Sciences, Tehran, Iran
Marquette University School of Dentistry, Milwaukee, WI
Biomaterials Group, Faculty of Biomedical Engineering, Amirkabir University of Technology, Tehran, Iran
Hossein E. Jazayeri[b]
Marquette University School of Dentistry, Milwaukee, WI
Lobat Tayebi
Marquette University School of Dentistry, Milwaukee, WI
Department of Engineering Science, University of Oxford, Oxford, UK

Materials Science and Engineering: C, Vol. 70, No. 1 (January 1, 2017): pg. 586-598. DOI. This article is © Elsevier and permission has been granted for this version to appear in e-Publications@Marquette. Elsevier does not grant permission for this article to be further copied/distributed or hosted elsewhere without the express permission from Elsevier.

NOT THE PUBLISHED VERSION; **this is the author's final, peer-reviewed manuscript.** The published version may be accessed by following the link in the citation at the bottom of the page.

Abstract: In this research, the three dimensional porous scaffolds made of a polycaprolactone (PCL) microsphere/TiO_2 nanotube (TNT) composite was fabricated and evaluated for potential bone substitute applications. We used a microsphere sintering method to produce three dimensional PCL microsphere/TNT composite scaffolds. The mechanical properties of composite scaffolds were regulated by varying parameters, such as sintering time, microsphere diameter range size and PCL/TNT ratio. The obtained results ascertained that the PCL/TNT (0.5 wt%) scaffold sintered at 60 °C for 90 min had the most optimal mechanical properties and an appropriate pore structure for bone tissue engineering applications. The average pore size and total porosity percentage increased after increasing the microsphere diameter range for PCL and PCL/TNT (0.5 wt%) scaffolds. The degradation rate was relatively high in PCL/TNT (0.5 wt%) composites compared to pure PCL when the samples were placed in the simulated body fluid (SBF) for 6 weeks. Also, the compressive strength and modulus of PCL and PCL/TNT (0.5 wt%) composite scaffolds decreased during the 6 weeks of storage in SBF. MTT (3-(4,5-Dimethylthiazol-2-yl)-2,5-Diphenyltetrazolium Bromide) assay and alkaline phosphates (ALP) activity results demonstrated that a generally increasing trend in cell viability was observed for PCL/TNT (0.5 wt%) scaffold sintered at 60 °C for 90 min compared to the control group. Eventually, the quantitative RT-PCR data provided the evidence that the PCL scaffold containing TiO_2 nanotube constitutes a good substrate for cell differentiation leading to ECM mineralization.

Keywords: PCL; TiO_2 nanotube; Scaffold; Tissue engineering; Mechanical properties

1. Introduction

Tissue engineering uses the basic principles of material technology and life science to restore the tissue integrity and functionality by replenishing cell density and activity along with encompassing gene expression and protein activity necessary for homeostatic maintenance of the initially damaged area.[1–20] Scaffolds are integral to this regenerative process.

PCL is one of the most critical thermoplastics and has received much consideration because of its adaptability, biodegradability, and applications in tissue engineering.[21] However, a few inadequacies, such as low melting temperature and low mechanical properties limit modern utilization of PCL. In order to enhance the physical properties of the polymer, inorganic particles were used to enhance a few its properties. The guarantee of these new composites is a controllable blend of the properties of the polymer (adaptability, toughness, and simple handling) and the properties of the filler (hardness, sturdiness and, thermal stability).[22]

Recently, TiO_2 particles have drawn more attention in the biomedical field. TiO_2 powders are effective in apatite formation on the PCL/TiO_2 composite surface in simulated body fluids (SBF), which is believed to be a prerequisite for bioactivity. Liu et al.[23] found that nano TiO_2 effectively enhanced cell attachment and proliferation. Goto et al.[24] similarly revealed that TiO_2-containing bone cement could not simply permit the regulation of the

Materials Science and Engineering: C, Vol. 70, No. 1 (January 1, 2017): pg. 586-598. DOI. This article is © Elsevier and permission has been granted for this version to appear in e-Publications@Marquette. Elsevier does not grant permission for this article to be further copied/distributed or hosted elsewhere without the express permission from Elsevier.

***NOT THE PUBLISHED VERSION;* this is the author's final, peer-reviewed manuscript.** The published version may be accessed by following the link in the citation at the bottom of the page.

setting time, and the handling of bone cement additionally enhances the osteoconductivity *in vitro* and *in vivo*. Nanosized titanium can also promote protein absorption and osteoblast adhesion.[24] Thus, nano-TiO_2 could be a potential material for bone repair applications. Nanomaterials are attractive for many applications since the reduction of the grain size to the nanometer scale can improve their physicochemical and mechanical characteristics.[25–58]

The ideal drug loading efficiency and the drug dosage optimization make a PCL microsphere an excellent carrier with controlled release. Borden et al.[59] developed a microsphere-sintered scaffold in which polymers, such as PLGA, were fabricated into microspheres by means of single emulsion techniques. By the action of heating and solvent, poly(lactic-*co*-glycolic acid) (PLGA) microspheres formed a scaffold with good mechanical properties. Compared to traditional methods, such as solvent casting/particulate leaching and thermally induced phase separation, the mechanical properties of the PLGA-sintered microsphere scaffold were remarkably improved.[59] Moreover, in addition to the advantages of the PCL microsphere, PCL-sintered microsphere scaffolds are also promising multifunctional vehicles for drug/protein delivery and tissue engineering.

In this study, PCL/TiO_2-sintered microsphere scaffolds were produced. The structural, mechanical and biological characterization of these composite scaffolds were evaluated.

The aim of this study was incorporation of TiO_2 nanotube into the PCL scaffold for improving mechanical properties (young modulus and compressive strength), biological properties (cell proliferation, bioactivity and MC3T3-E1 pre-osteoblast differentiation) and physicochemical properties (hydrophilicity) for bone tissue engineering applications.

2. Experimental procedure

2.1. Synthesis of TNTs

The TiO_2 precursor employed for synthesis of nanotube was a commercially obtainable TiO_2 powder (P25, Degussa AG) with crystalline structure of rutile and anatase and with a primary particle size of 21 nm. For TNT preparation, briefly, 1.14 g of P25 powder treated with 40–45 mL of 10 N NaOH solution in a Teflon-lined autoclave at temperature of 150 °C for 48 h. The obtained precipitates after the hydrothermal treatment were adequately washed with de-ionized water and HCl aqueous solution (1 M) and was

Materials Science and Engineering: C, Vol. 70, No. 1 (January 1, 2017): pg. 586-598. DOI. This article is © Elsevier and permission has been granted for this version to appear in e-Publications@Marquette. Elsevier does not grant permission for this article to be further copied/distributed or hosted elsewhere without the express permission from Elsevier.

NOT THE PUBLISHED VERSION; **this is the author's final, peer-reviewed manuscript.** The published version may be accessed by following the link in the citation at the bottom of the page.

subsequently separated from the washing solution by filtration while the pH value of the rinsing solution was < 7. Finally, the powders were dried at 80 °C for 3 h.

2.2. PCL/TNT composite scaffold

2.2.1. Preparation of PCL/TNT microspheres

PCL/TNT composite microspheres were prepared using a modification of the emulsion and solvent evaporation method. In brief, PCL (Art No. 704,105; M_w = 48,000–90,000 Da; Sigma-Aldrich) was dissolved in methylene chloride (Merck Co.) to make a 24% (w/v) solution. To make PCL/TNT microspheres with a certain PCL to TNT ratio, a known amount of TNT (0, 0.5, 1.25 and 2.5 wt%) powders (were synthesized and characterized in our previous works[60,61]) were dispersed in this solution by agitating on a magnetic stirrer for 2 h. The solution was then poured into a 0.25% Poly(vinyl alcohol) (PVA) (M_w = 13,000–23,000 Da; Sigma-Aldrich) solution stirring at 500 rpm at room temperature. Then, the microspheres were filtered and washed with de-ionized water to remove possible traces of organic solvent and dried in a freeze-drier system (Alpha 1–2 LD, Germany) for 10 h. Microspheres were separated selectively into the following size ranges by using commercial sieves, 300–500 μm and 500–1000 μm.

2.2.2. Preparation of PCL/TNT composite scaffolds

The three-dimensional (3D) composite scaffolds were prepared by a sintered microsphere method. For this purpose, the PCL/TNT microspheres obtained by single emulsion technique, with 300–500 and 500–1000 μm size range were packed tightly into a stainless mold and heated at 60 °C in an oven (see Fig. 4) for 60 and 90 min, respectively. The scaffold obtained was then allowed to cool down to room temperature and finally was removed from the mold.

2.3. Characterization of PCL/TNT composite scaffolds

2.3.1. SEM observations

The microstructure and morphology of the porous composite scaffold was evaluated using scanning electron microscopy (SEM). The scaffold sample was coated with a thin layer of gold (Au) by sputtering (EMITECH K450X, England), and then, the morphology of it was observed on a scanning electron microscope (SEM—Tescan Vega 2XMU) that operated at the acceleration voltage of 10 kV.

Materials Science and Engineering: C, Vol. 70, No. 1 (January 1, 2017): pg. 586-598. DOI. This article is © Elsevier and permission has been granted for this version to appear in e-Publications@Marquette. Elsevier does not grant permission for this article to be further copied/distributed or hosted elsewhere without the express permission from Elsevier.

***NOT THE PUBLISHED VERSION;* this is the author's final, peer-reviewed manuscript.** The published version may be accessed by following the link in the citation at the bottom of the page.

2.3.2. Mechanical properties

The compressive strength and modulus of the composite scaffolds were measured using a mechanical testing machine (SMT-20, Santam, Iran). According to ASTM D695–15 standard, cylindrical samples with length-to-diameter ratio of 2:1 (10 mm in length and 5 mm in diameter) were prepared. The cross-head speed was set at 0.5 mm/min, and the load was applied until the specimen was compressed to approximately 30% of its original length. The elastic modulus was determined as the slope of the initial linear portion of the stress–strain curve. The compressive strength was calculated as the maximum point of the stress–strain curve.

2.3.3. Biodegradation test

Scaffolds were weighed once prior to the degradation study, and once again after the following time points: 0 week, 1 week, 2 weeks, 3 weeks, 4 weeks, 5 weeks and 6 weeks. At each time point, samples were removed from SBF, rinsed twice with deionized water, and lyophilized for 48 h to ensure the complete removal of water, and weighed. The weight loss percentages of the specimens were calculated from the weights obtained before and after degradation as below:

$$\text{Weightloss}(\%) = (W_1 - W_2)/W_1 \times 100 \quad (1)$$

where W_1 and W_2 are the sample weight before and after degradation, respectively.

2.3.4. Mercury intrusion porosimetry analysis

The total volume of mercury forced into the sample enables the calculation of the overall porosity, while the mercury volume variation measured at each pressure interval permits for the calculation of pore size using the Washburn equation:

$$\mathrm{P} \times r = -2\gamma \times cos\theta \quad (2)$$

where p is the applied pressure, r is the radius of the pore, γ is the surface tension of the mercury and θ is the contact angle between mercury and the scaffold. The weight of the sample in the glass holder was determined both before and after the introduction of mercury. The difference in weight divided by the density of mercury at room temperature gives the total volume used. By dividing the total pore volume by the external volume of the sample, the porosity or percent pore volume was calculated. Finally, a built-in algorithm was employed to automatically calculate pore size at each pressure interval so that the pore size distribution was obtained once all the points were recorded.

Materials Science and Engineering: C, Vol. 70, No. 1 (January 1, 2017): pg. 586-598. DOI. This article is © Elsevier and permission has been granted for this version to appear in e-Publications@Marquette. Elsevier does not grant permission for this article to be further copied/distributed or hosted elsewhere without the express permission from Elsevier.

***NOT THE PUBLISHED VERSION;* this is the author's final, peer-reviewed manuscript.** The published version may be accessed by following the link in the citation at the bottom of the page.

2.3.5. In vitro *biological evaluation*

2.3.5.1. Cell culture

Osteoblast cell lines were cultured in Dulbecco's Modified Eagle Medium (DMEM, Gibco, USA) containing 10% fetal bovine serum, 1% penicillin – streptomycin, 0.25 mg/mL fungizone, and 2 mM l-glutamine. The culture medium was replaced every 2 days and cultures were maintained in a humidified incubator at 37 °C with 5% CO_2. Then, after about 80% confluence, the cells were digested and subcultured using 0.25% (w/v) trypsin-ethylenediamineteraacetic acid. The resulting cells in a suspension were then seeded separately onto scaffolds that had been sterilized by ^{60}Co g-irradiation. For control experiments, polystyrene tissue culture plates (TCPs) were employed. The cells were seeded onto each sample by dripping a cell suspension in 24-well plate, and then, the culture wells were filled with 1 mL of culture medium after 2 h in the incubator.

2.3.5.2. MTT assay

The cell proliferation on the nanocomposite scaffolds was determined using the MTT (3-(4,5-dimethylthiazol-2-yl)-2,5-diphenyltetrazolium bromide) assay. For the assay, cells (G-292) were then seeded onto 96-well plates at a density of 2×10^4 cells/well and were incubated under standard culturing conditions. The cells were seeded onto the PCL and PCL/TNT scaffolds after an overnight incubation at 37 °C with 5% CO_2 in a humidified atmosphere. Three wells in the absence of scaffolds were used as negative controls [tissue culture polystyrene (TCPS)]. For each sample, five wells of microliter plate were selected. The plates were incubated for 3, 7, and 14 days with a half media changed every 2 days. Then, nanocomposite scaffolds were removed from the wells and 10 μL of a 5 mg/mL solution of MTT was added to each well followed by incubation for 5 h at 37 °C. Formed formazan crystals were dissolved by the addition of 100 μL/well of isopropanol. Subsequently, the plates were incubated at 37 °C for 10 min and transferred to 48 °C for 15 min before absorbance measurements. Optical density (OD) was recorded on a multiwell microplate reader at a wavelength of 570 nm.

2.3.5.3. ALP activity

The functional activity of the cells on the prepared scaffolds was evaluated by measuring the ALP activity. ALP activity was conducted using a commercial kinetics method. Briefly, the G-292 cell were transferred into 24-well microliter plates at 2×10^4 cells/well, separately. The PCL and PCL/TNT scaffolds were placed in the wells. Three wells in the absence of the scaffolds were used as negative controls [tissue culture polystyrene

Materials Science and Engineering: C, Vol. 70, No. 1 (January 1, 2017): pg. 586-598. DOI. This article is © Elsevier and permission has been granted for this version to appear in e-Publications@Marquette. Elsevier does not grant permission for this article to be further copied/distributed or hosted elsewhere without the express permission from Elsevier.

***NOT THE PUBLISHED VERSION;* this is the author's final, peer-reviewed manuscript.** The published version may be accessed by following the link in the citation at the bottom of the page.

(TCPS)]. The plates were incubated for 3, 7 and 14 days at 37 °C in humidified air with 5% CO_2. Approximately 10 μL of the supernatant was removed from each well at 3, 7 and 14 days and processed according to the guideline. It is notable that the color changing was measured by a spectrophotometer at 405 nm. The standard *p*-nitrophenol curve was employed to convert the obtained absorbance data to the ALP content.

2.3.5.4. qRT-PCR analysis

The expression levels of osteogenesis-related genes were assessed utilizing the quantitative reverse transcription-polymerase chain reaction (qRT-PCR). The MC3T3-E1 cells were seeded at a density of 2×10^4 cells/well, cultured for 3 and 7 days, and then harvested employing TRIzol to extract RNA. An equivalent amount of RNA from each scaffold was reverse-transcribed into complementary DNA (cDNA) by using the Superscript II first-strand cDNA synthesis kit. Finally, the qRT-PCR analysis of osteocalcin (OCN), Type I collagen (COL-1) and Runt-related transcription factor 2 (RUNX-2) genes was conducted.

2.3.5.5. SEM observations of cell morphology

Cells cultured on the prepared 3D scaffolds were fixed with glutaraldehyde (2.5% in PBS) for 45 min. Sample dehydration was conducted by slow water replacement employing series of ethanol solutions (30, 50, 70, 90%) for 15 min with a final dehydration in absolute ethanol for 30 min, permitting specimens to dry at ambient temperature and under vacuum. Subsequently, the pieces were mounted on stubs and coated in vacuum with gold (Au).

2.4. Statistical analysis

All data values are presented as mean ± standard deviation for each group of samples. For the mechanical and biological properties, five samples were tested per group. A paired sample *t*-test and one-way analysis of variance (ANOVA) was performed to determine statistically significant differences between groups. If ANOVA detected a significant difference within the data set, Tukey's honestly significantly different (HSD) multiple comparison test was used to determine significant differences between sample groups. All tests were conducted with 95% confidence intervals (p value < 0.05).

Materials Science and Engineering: C, Vol. 70, No. 1 (January 1, 2017): pg. 586-598. DOI. This article is © Elsevier and permission has been granted for this version to appear in e-Publications@Marquette. Elsevier does not grant permission for this article to be further copied/distributed or hosted elsewhere without the express permission from Elsevier.

***NOT THE PUBLISHED VERSION;* this is the author's final, peer-reviewed manuscript.** The published version may be accessed by following the link in the citation at the bottom of the page.

3. Results & discussion

3.1. Titania nanotubes

The crystallinity and the phase changes of synthesized specimens after hydrothermal process at 150 °C in comparison with P25 particle were examined by XRD analysis (see Fig. 1). All peaks in the XRD pattern of P25 was indistinguishable to the beginning raw materials, which is, comprises of mixed anatase and rutile titania phase which were depicted with the sharp peaks. It is noticeable that one-dimensional (1D) titanate structure is available after treating up to 150 °C rise of another, broad and low angle peak between 5 and 10° (main peak of TNT structure) that displaying the conversion anatase and rutile peaks to a new phase that is attributed to the layered wall titanate structure.[60,61]

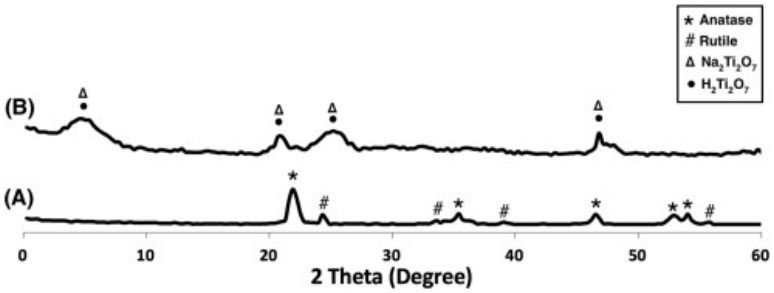

Fig. 1. XRD Patterns of (a) starting powder P25 and (b) synthesized 1D titanates.

XRD pattern additionally displayed predominantly four diffraction peaks at 2θ ~ 5.5, 24, 28 and 48° features for $Na_2Ti_3O_7$ or $H_2Ti_3O_7$ type of titanate (JCPDS 31–1329) (JCPDS 41–192), respectively that having a monoclinic crystalline structure, and is made out of corrugated strips of edge-sharing TiO_6 octahedral, each strip is three-octahedral wide and strips further corner join to form stepped layers. The mentioned peaks could be related to the interlayer spacing typical for 1D titanate structure.[62,63] Thus, the chemical structure of the synthesized TNTs in this research could be $Na_xH_{2-x}Ti_3O_7$.

3.2. Before soaking in SBF

3.2.1. SEM observations

Fig. 2 shows SEM micrographs of microspheres produced by the single emulsion method with different sizes. The microspheres resulted in spherical morphologies, and their surfaces appeared rough and not porous.

Materials Science and Engineering: C, Vol. 70, No. 1 (January 1, 2017): pg. 586-598. DOI. This article is © Elsevier and permission has been granted for this version to appear in e-Publications@Marquette. Elsevier does not grant permission for this article to be further copied/distributed or hosted elsewhere without the express permission from Elsevier.

***NOT THE PUBLISHED VERSION;* this is the author's final, peer-reviewed manuscript.** The published version may be accessed by following the link in the citation at the bottom of the page.

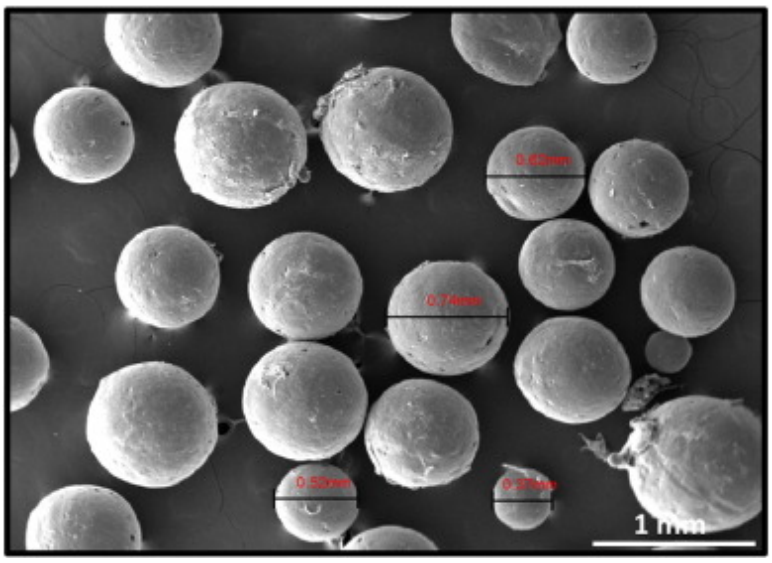

Fig. 2. SEM micrographs of PCL microspheres obtained by single emulsion method.

The optimized processing conditions (60 °C for 90 min) were suitable for sintered microsphere-based scaffolds with a well-defined 3D micro-structure, as presented in the micrographs of Fig. 3. The microscopic analysis also demonstrated that microspheres are randomly packed together with connecting necks arranged uniformly along the spatial dimension.

Materials Science and Engineering: C, Vol. 70, No. 1 (January 1, 2017): pg. 586-598. DOI. This article is © Elsevier and permission has been granted for this version to appear in e-Publications@Marquette. Elsevier does not grant permission for this article to be further copied/distributed or hosted elsewhere without the express permission from Elsevier.

***NOT THE PUBLISHED VERSION;* this is the author's final, peer-reviewed manuscript.** The published version may be accessed by following the link in the citation at the bottom of the page.

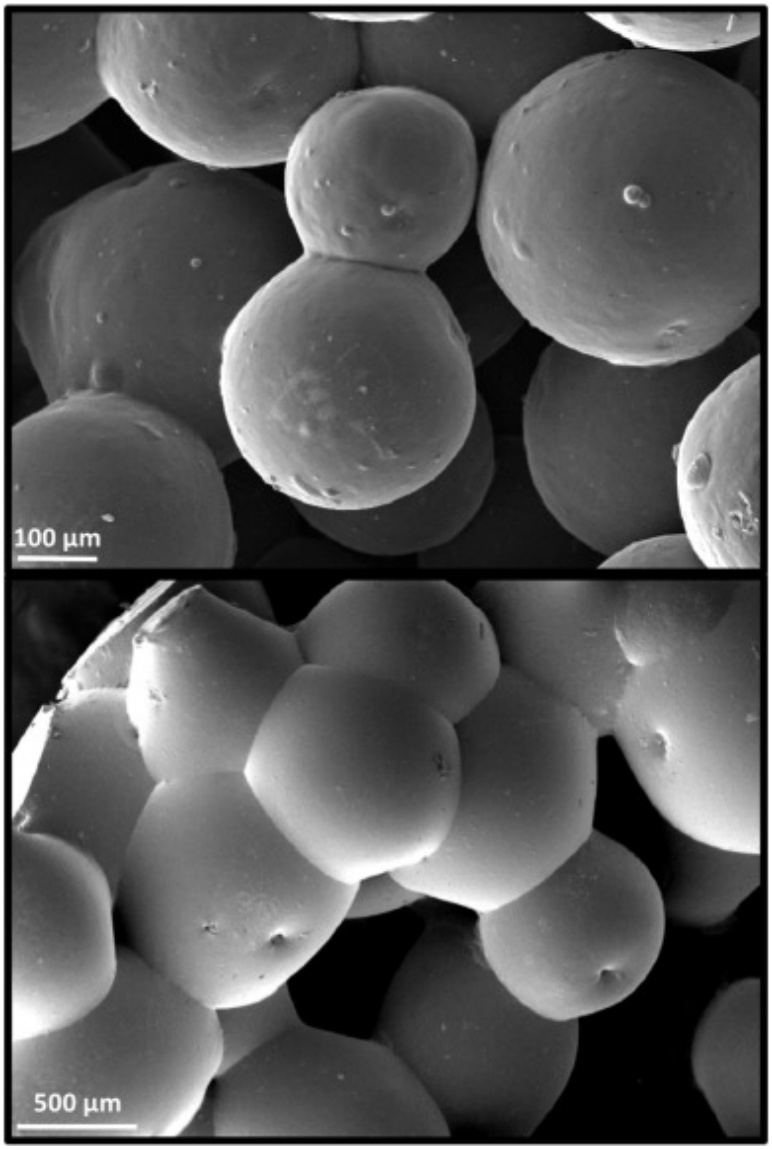

Fig. 3. SEM micrograph of PCL/TNT (0.5 wt%) composite scaffolds sintered at 60 °C, for 90 min at different magnifications.

As it can be observed in this figure, the SEM micrograph of PCL/TNT microsphere scaffolds sintered at 60 °C for 90 min. The scaffolds were made by microspheres, and all types of PCL-based microspheres remained in spherical shape with visible rough surfaces because of great TNT conglomeration enrichment on their surfaces.

Materials Science and Engineering: C, Vol. 70, No. 1 (January 1, 2017): pg. 586-598. DOI. This article is © Elsevier and permission has been granted for this version to appear in e-Publications@Marquette. Elsevier does not grant permission for this article to be further copied/distributed or hosted elsewhere without the express permission from Elsevier.

***NOT THE PUBLISHED VERSION;* this is the author's final, peer-reviewed manuscript.** The published version may be accessed by following the link in the citation at the bottom of the page.

3.2.2. Mechanical properties

The preparation of 3D porous composite scaffolds is achievable through a microsphere sintering technique. The sintering time is the processing parameter that can control the mechanical properties and porous structures of the sintered microsphere scaffolds. Figs. 4 and 5 show the measured compressive modulus and strength of the composite scaffolds for different size ranges sintered (300–500 μm and 500–1000 μm) under different conditions. As it can be seen in this figure, the compressive modulus and compressive strength of the PCL/TNT (0.5 wt%) scaffolds sintered at 60 °C for 90 min (3.65 ± 0.18 MPa for 300–500 μm and 3.2 ± 0.16 MPA for 500–1000 μm) are remarkably and statistically higher than the scaffolds prepared at other sintering conditions (p value < 0.05). Increasing either sintering time resulted in better mechanical properties because of a greater bonding area. Also, by increasing the TNT in the composite scaffold, the mechanical properties decrease.

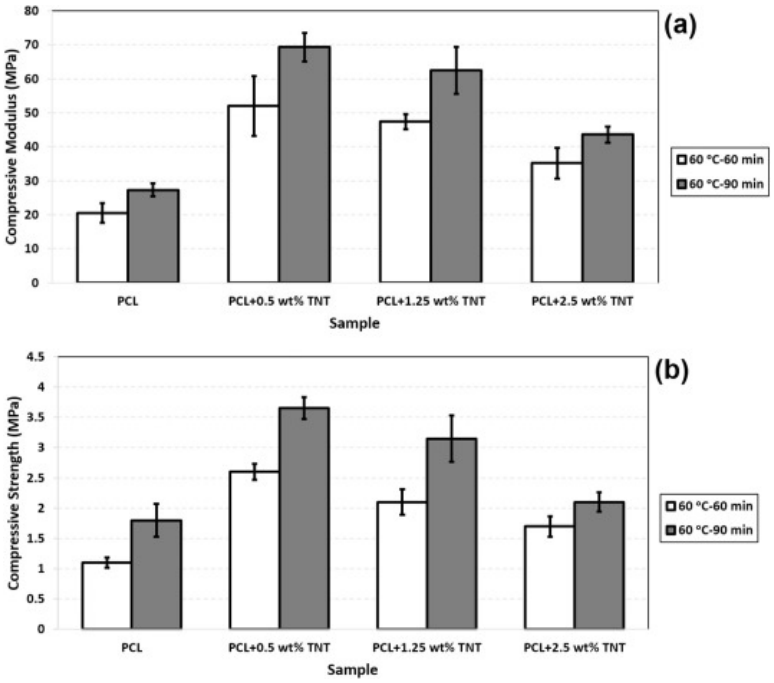

Fig. 4. (a) Compressive modulus and (b) compressive strength of the scaffolds as a function of scaffold compositions and sintering conditions (microsphere range size: 300–500 μm) ($n = 5$).

Materials Science and Engineering: C, Vol. 70, No. 1 (January 1, 2017): pg. 586-598. DOI. This article is © Elsevier and permission has been granted for this version to appear in e-Publications@Marquette. Elsevier does not grant permission for this article to be further copied/distributed or hosted elsewhere without the express permission from Elsevier.

***NOT THE PUBLISHED VERSION;* this is the author's final, peer-reviewed manuscript.** The published version may be accessed by following the link in the citation at the bottom of the page.

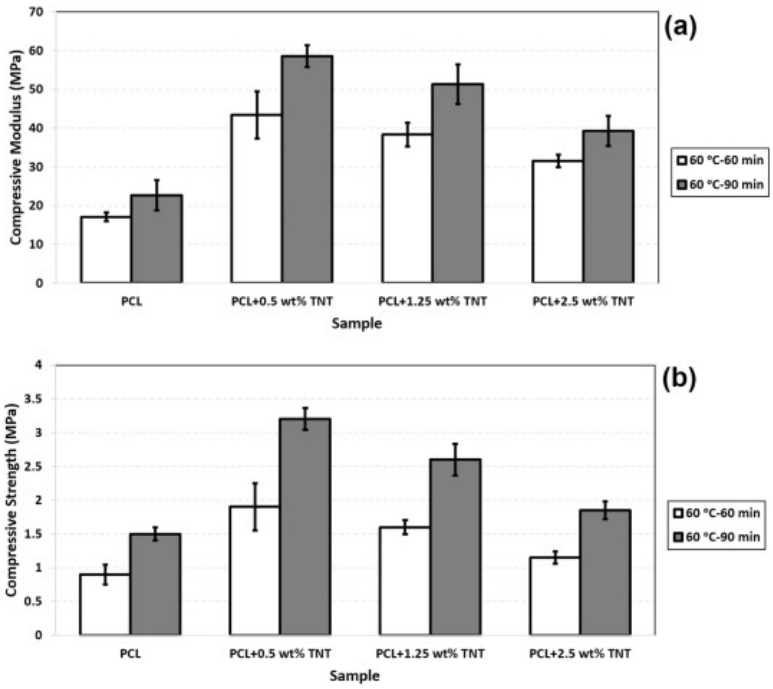

Fig. 5. (a) Compressive modulus and (b) compressive strength of the scaffolds as a function of scaffold compositions and sintering conditions (microsphere range size: 500–1000 μm) (n = 5).

The compressive modulus and compressive strength increase at a decreasing microsphere diameter range. In particular, the data showed that a decrease in microsphere size range (from 500–1000 to 300–500 μm) resulted in an increase in the compressive modulus. This could be attributed to the increase in the number of connecting necks between microspheres at smaller size ranges. Moreover, PCL/TNT (0.5 wt%) showed a statistically higher compressive modulus (69.3 ± 4.2 MPa for 300–500 μm and 58.6 ± 2.8 MPA for 500–1000 μm) and compressive strength compared to other prepared scaffolds (p value < 0.05), and therefore, this scaffold was selected as an optimum sample for further evaluation of mechanical properties. Loadings beyond 0.5 wt% TNT in the starting material led to a decrease in the mechanical properties of these prepared scaffolds, due in part to the aggregation of nanotubes. In addition, the upgrade in compressive modulus and compressive strength at smaller microsphere diameters could be ascribed to the reduction in the porosity of the scaffolds. From the aforementioned discussion, it can be concluded that the TiO_2 nanotube can act as an excellent reinforcing agent for a PCL matrix in order to produce a new generation of bone tissue engineering scaffolds. However, scaffolds with mechanical properties falling in the proposed range are still reasonable for tissue engineering applications as they are within the range of trabecular bone (0.01–2.0 GPa), as confirmed by several researchers.[64] A point-by-point quantitative investigation of porosity features was carried out in order to measure the impact of sintering time and

Materials Science and Engineering: C, Vol. 70, No. 1 (January 1, 2017): pg. 586-598. DOI. This article is © Elsevier and permission has been granted for this version to appear in e-Publications@Marquette. Elsevier does not grant permission for this article to be further copied/distributed or hosted elsewhere without the express permission from Elsevier.

***NOT THE PUBLISHED VERSION;* this is the author's final, peer-reviewed manuscript.** The published version may be accessed by following the link in the citation at the bottom of the page.

microsphere sizes on the pore size and percentage of interconnected porosity of the sintered microspheres.

In fact, the leading factor in microsphere sintering scaffold preparation is the control over the degree of bonding among the microspheres by finely regulating sintering conditions. A small bonding area results in weak coalescence among microspheres, leading to poor mechanical characteristics of the scaffold, while a large bonding area leads to a reduction in scaffold porosity and interconnection.

The need for alternatives to currently available bone graft substitutes has generated numerous candidates, many of which are composed of a polymer and ceramic. The use of this combination is well-founded as titanium dioxide (TiO_2) is the inorganic material and has been shown to be bioactive, osteoconductive and, in some instances, osteoinductive.

In the present paper, we designed and prepared PCL/TNT composite sintered microsphere scaffolds for applications in bone tissue engineering. The underlying hypothesis is that the incorporation of TNT can improve the mechanical properties of the polymeric (PCL) scaffolds and thereby generate better matrices for bone tissue engineering applications.

The mechanical properties were shown to be dependent on a number of parameters, including polymer/ceramic ratio within the microspheres, and heating time of the matrix.

As the bond increases with longer heating times, the strength of the matrix increases as well. However, as the heating time increases, the risk of microspheres fusing together increases as well. As the bond between neighboring microspheres increases, it is more likely that pores that are formed between adjacent microspheres will be closed off, weakening the interconnected pore structure of the matrix. Thus, it is beneficial to increase the heating to obtain stronger compressive properties.[65]

Equally important to mechanical properties is the surface area available for microsphere-microsphere bonding. To bond the microspheres together, the composite matrix is heated above the glass transition temperature (T_g) of the polymer. By heating above the T_g, the polymeric chains become energized and begin to intertwine with those of the neighboring microspheres. As more time passes, the extent of intertwining increases and the bond is enhanced. However, this can only take place if the two surfaces in contact with each other are polymeric. In the instance that the TiO_2 nanotube is available on the

Materials Science and Engineering: C, Vol. 70, No. 1 (January 1, 2017): pg. 586-598. DOI. This article is © Elsevier and permission has been granted for this version to appear in e-Publications@Marquette. Elsevier does not grant permission for this article to be further copied/distributed or hosted elsewhere without the express permission from Elsevier.

***NOT THE PUBLISHED VERSION;* this is the author's final, peer-reviewed manuscript.** The published version may be accessed by following the link in the citation at the bottom of the page.

surface and is in contact with either polymer or TiO_2 nanotube on the neighboring microsphere, bonding will not take place. Rather, to sinter TiO_2, the temperature would need to be heated to several hundred degrees C, which would remove the polymer (PCL) completely. As the polymeric content of the microsphere decreases and the potential for TiO_2 to be on the surface of the microsphere increases, the bonds between microspheres will decrease and the matrix will lose mechanical properties. Thus, it can be inferred that as the polymer/ceramic ratio decreases, the mechanical properties of the matrix will also decrease. As the polymer content of the microspheres increases, and therefore surfaces available for bonding increases, the mechanical properties also increase.[65]

The realization of scaffolds *via* a bottom-up approach based on microsphere assembly offers several advantages compared to conventional techniques of porous scaffold preparation.

In particular, it permits the independent control over pore size, interconnection, mechanical characteristics and additionally customized arrival of multiple bioactive signals. Hence, the usage of new methodologies based on the assembly of microspheres represents a fundamental outline stage to control spatial properties and the worldly development of scaffold properties, which is required to direct the microanatomical arrangement of complex tissues, such as bone. Here, we suggest a strategy that allows for the sintering of microspheres with unexpected morphological and structural properties through chemical and thermal route to engineer a synthetic scaffold that would give a negative layout for bone regeneration.[64]

3.2.3. Mercury intrusion porosimetry

Fig. 6 compares porosity data obtained by mercury intrusion porosimetry from the prepared scaffold in order to determine a relationship among microsphere size range and porosity features (*i.e.*, pore size, pore fraction). The average pore size and total porosity percentage increased at an increasing microsphere diameter range for both prepared scaffolds (see Fig. 15) (36 ± 5 for PCL + 0.5 wt% TNT for 300–500 μm and 33 ± 4 for 500–1000 μm)(p value > 0.05). Also, the pore structures of the composite scaffolds are affected by sintering conditions. Tahriri and Moztarzadeh[11] reported that increasing sintering time resulted in possible closure of pores, which led to decreased scaffold porosity. Also, Luciani et al.[64] exhibited that the average pore size increased after enhancing microsphere diameters. Therefore, the suggested methodology fulfills the idea that bottom-up approaches allow for the prediction of macropore size by properly choosing the microsphere diameter range.

Materials Science and Engineering: C, Vol. 70, No. 1 (January 1, 2017): pg. 586-598. DOI. This article is © Elsevier and permission has been granted for this version to appear in e-Publications@Marquette. Elsevier does not grant permission for this article to be further copied/distributed or hosted elsewhere without the express permission from Elsevier.

***NOT THE PUBLISHED VERSION;* this is the author's final, peer-reviewed manuscript.** The published version may be accessed by following the link in the citation at the bottom of the page.

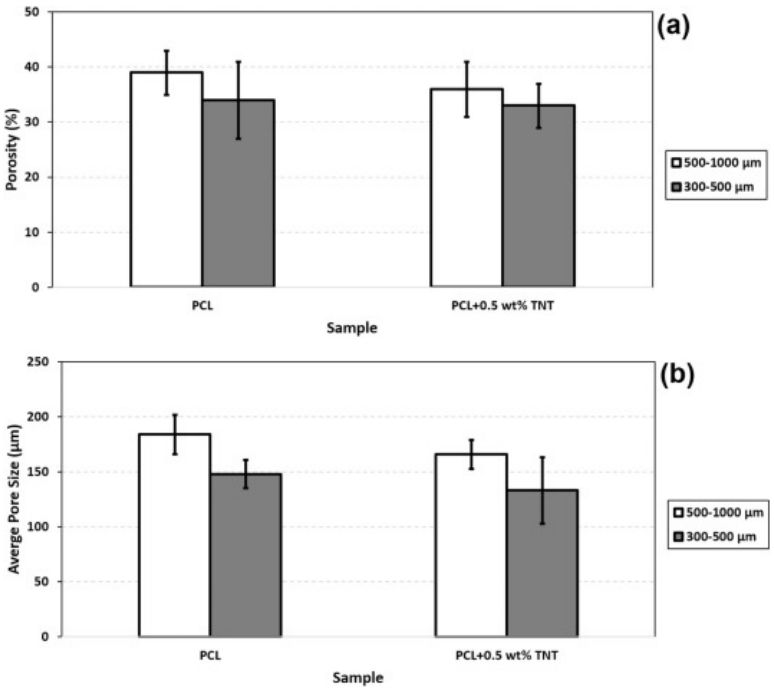

Fig. 6. Evaluation of porosity features by mercury intrusion porosimetry (a) total porosity and (b) average pore diameter of the prepared scaffolds as a function of scaffold composition and microspheres diameter range (n = 5).

The porosity of PCL/TNT scaffolds was affected by sintering conditions as well. This observation is in agreement with what Jiang et al. found previously.[66]

The sintered microsphere technique of constructing scaffolds is to pack microspheres in a confined 3D space, which guarantees the interconnected pore structure because of the nature of the geometry. The natural bone is composed of approximately 30% tissue and 70% pore volume.[67] The development aim of sintered microsphere technique is to prepare a negative template for bone regeneration,[68,69] it means that, a 3D matrix with approximately 30% pore volume and 70% biodegradable scaffolding materials. Apparently, 30% pore volume will be filled with newly formed bone tissue and the remaining percentage constituting degradable biomaterials (70%) will be absorbed by human body.[70] Therefore, this structure could itself be utilized as a scaffold, or as synthetic scaffold providing a negative template for bone regeneration.[69]

Many scaffold preparation techniques, such as gas foaming[71] and phase separation/leaching technique,[72] give rise to scaffolds with high porosity. However, the mechanical properties of these obtained scaffolds can often be compromised and can be as low as < 1 MPa.[71] The porosity should always be balanced with the mechanical need of the

Materials Science and Engineering: C, Vol. 70, No. 1 (January 1, 2017): pg. 586-598. DOI. This article is © Elsevier and permission has been granted for this version to appear in e-Publications@Marquette. Elsevier does not grant permission for this article to be further copied/distributed or hosted elsewhere without the express permission from Elsevier.

NOT THE PUBLISHED VERSION; **this is the author's final, peer-reviewed manuscript.** The published version may be accessed by following the link in the citation at the bottom of the page.

scaffolds. Thus, the porosity (~ 35%) of the PCL/TNT (0.5 wt%) scaffold sintered at 60 °C for 90 min is appropriate, considering the scaffold's role as a negative template and the highest mechanical property the scaffolds displayed.

The initial work by Hulbert et al.[73] demonstrated that the minimum pore size for significant ingrowth of natural bone was between 75 and 100 μm. Many researchers have reported a pore size above 100 μm for defining a narrower range of optimal values. Klenke et al.[74] reported the effect of pore size on vascularization and osseointegration of biphasic calcium phosphate particles in critical-sized cranial defects in mice. It is reported that the functional capillary density was remarkably higher with ceramic particles with pore sizes > 140 μm than those whose pore sizes were < 140 μm. In addition, the volume of newly formed bone increased as pore size increased and the group with pore size of 210–280 μm exhibited the highest degree of bone formation. In another study by Gotz et al.,[75] the amount of lamellar bone formation was found to be linearly related to pore size. In 100 μm pores, bone remodeling took place with a pronounced time lag as compared to larger pores. In 300 μm pores, a delayed osseointegration was seen as compared to 200 μm pores. Therefore, they concluded that 200 μm may be the optimum pore size for laser-textured Ti6A14V implants. Considering these findings in the literature, the pore size of approximately 150 μm for 300–500 μm and 185 μm for 500–1000 μm of our PCL/TNT (0.5 wt%) composite scaffolds sintered at 60 °C for 90 min should be appropriate for bone regeneration.

3.3. After soaking in SBF

3.3.1. Biodegradation test

The biodegradation behavior of PCL and its composites have been examined for six weeks. Weight loss has been conducted as a measure of biodegradation when the samples were soaked in the SBF. Fig. 7 shows the weight loss of pure PCL and its composites as a function of time. It is clear that the degradation rate is entirely rapid in composites as compared to pure PCL.

Materials Science and Engineering: C, Vol. 70, No. 1 (January 1, 2017): pg. 586-598. DOI. This article is © Elsevier and permission has been granted for this version to appear in e-Publications@Marquette. Elsevier does not grant permission for this article to be further copied/distributed or hosted elsewhere without the express permission from Elsevier.

***NOT THE PUBLISHED VERSION;* this is the author's final, peer-reviewed manuscript.** The published version may be accessed by following the link in the citation at the bottom of the page.

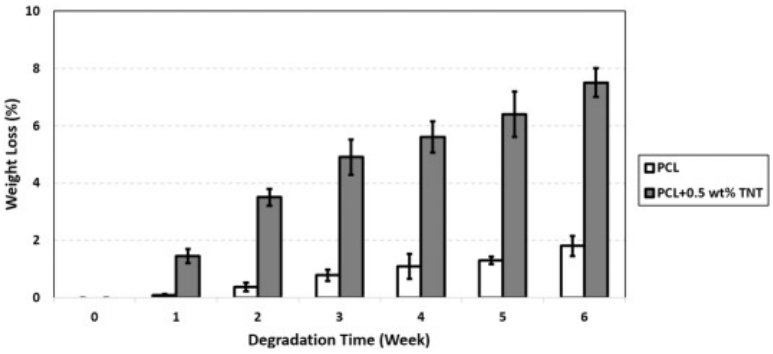

Fig. 7. Weight loss of prepared scaffolds in SBF as a function of time (n = 5)).

On the other hand, the composite with TNT exhibits greater degradation than that of the pure PCL [(1.45 ± 0.24% for 1 week and 7.5 ± 0 5% for 6 weeks for PCL + 0.5 wt% TNT) and (0.095 ± 0.02% for 1 week and 1.8 ± 0.35% for 6 weeks for pure PCL)] (p value < 0.05). Initially, due to the swelling of the polymer, degradation was slower, but as the time increased, weight losses were observed. Much less deterioration was seen for pure PCL while composites exhibit approximately huge degradation. For a biodegradable polyester like PCL, the degradation happens *via* hydration following the hydrolysis of ester linkages. The rate of chain scission is connected with its crystallinity since cleavage occurs overwhelmingly in the amorphous section of the polymer.[76]

It is noticeable that PCL is less hydrophilic and highly crystalline than its various composites. Also, rapid water penetration is not allowed in the PCL due to its hydrophobicity in nature. Furthermore, the PCL/TNT composite has a higher surface area and has better water adsorbability. Therefore, the composites exhibit a higher degradation rate in comparison to pure PCL. Biodegradation and mineralization of PCL/TNT composite is faster and greater as compared to pure PCL. Therefore, PCL/TNT composite is a superior material for bioimplants and other biomedical applications where a smaller dimension and higher surface area of TiO_2 nanotube could enhance the characteristics of the composite.

The degradation of a scaffold is perhaps the most important feature in designing a scaffold. We previously discussed the importance of tailoring a scaffold's properties to match the mechanical properties of the tissue it was restoring. An ideal scaffold would establish a biochemical and mechanical support system until the damaged tissue was fully regenerated. A perfect scaffold would biodegrade at a rate steady and in accordance with tissue regeneration. This prevents pseudohealing, in which the scaffold has completely degraded but the tissue regenerated is not yet at full functionality. In addition, scaffold biodegradation that is slower than tissue regeneration could inhibit or disrupt new tissue functionality. Similarly, as it essential to the achievement of an orthopedic scaffold, a layer

Materials Science and Engineering: C, Vol. 70, No. 1 (January 1, 2017): pg. 586-598. DOI. This article is © Elsevier and permission has been granted for this version to appear in e-Publications@Marquette. Elsevier does not grant permission for this article to be further copied/distributed or hosted elsewhere without the express permission from Elsevier.

***NOT THE PUBLISHED VERSION;* this is the author's final, peer-reviewed manuscript.** The published version may be accessed by following the link in the citation at the bottom of the page.

of calcium phosphate mineralization occurs on its surface. The coating of calcium phosphate on an implant has been displayed to increase its ability to bond *in vivo* with native bone.[77] The accomplishment of an orthopedic implant is intrinsically connected to its capacity to attach to local bone *in vivo*. This bonding promotes osseointegration, the formation of a direct interface between an implant and bone, without intervening soft tissue.[78,79]

The encapsulation of orthopedic implants by fibrous tissue is very much demonstrated and is one of the main sources of implant failure. Implant loosening is an indirect result usually due to mechanical or wear debris causing fibrous tissue to isolate the implant from the native bone. While surface properties, such as surface roughness, surface chemistry and topography play an important role in developing strong osseointegration, so does a surface layer of calcium phosphate mineralization.[79–82] Nonetheless, there are differing speculations on how bone (mineralized or not) re-precipitates. It is proposed that uncovered phosphate (PO_4^{3-}) and hydroxyl groups ($-$ OH) from the mineral layer evoke a negative charge[83,84] on the surface of the material. This attracts the positively charged calcium ions, leeched from the bone, to the surface of the bone. This then attracts the negatively charged phosphate ions, which results in re-precipitation on the surface. This is known as heterogeneous nucleation. The link between a calcium phosphate layer on a scaffold's surface and the osseointegration of the scaffold and native bone is well ascertained. Thus, it is evident that the ability of a scaffold to form a calcium phosphate layer on its surface is paramount to developing an effective and functional scaffold *in vivo*.

In our degradation studies, the scaffolds were immersed in SBF. The ionic concentration of the SBF was similar to that of human plasma. In addition, SBF was used to decide bioactivity - to be specific, calcium phosphate deposition - on the surface of the scaffolds. Specifically, we assessed whether the addition of the TNT in a scaffold's composition would enhance the calcium phosphate mineralization on its surface.

3.3.2. Mechanical properties

The compressive modulus and compressive strength of the prepared scaffolds after immersion in SBF are shown in Fig. 8 and 9 as a function of immersion time, respectively. The compressive strength and modulus of PCL and PCL/TNT composite scaffolds decreased during the 6 weeks. The compressive strength of PCL and PCL/TNT scaffolds decreased from the as-fabricated value of 1.8 ± 0.27 MPa to 1.27 ± 0.12 MPa and 3.65 ± 0.18 MPa to 2.55 ± 0.12 MPa after 6 weeks in SBF, respectively (p value < 0.05). Furthermore, the compressive modulus of PCL and PCL/TNT scaffolds decreased from the

Materials Science and Engineering: C, Vol. 70, No. 1 (January 1, 2017): pg. 586-598. DOI. This article is © Elsevier and permission has been granted for this version to appear in e-Publications@Marquette. Elsevier does not grant permission for this article to be further copied/distributed or hosted elsewhere without the express permission from Elsevier.

***NOT THE PUBLISHED VERSION;* this is the author's final, peer-reviewed manuscript.** The published version may be accessed by following the link in the citation at the bottom of the page.

as-fabricated value of 27.3 ± 1.9 MPa to 23.6 ± 0.95 MPa and 69.3 ± 4.2 MPa to 57.4 ± 2.9 MPa after 6 weeks in SBF, respectively (p value < 0.05). Therefore, both types of the prepared scaffolds approximately maintained the compressive mechanical properties during 6 weeks of *in vitro* degradation.

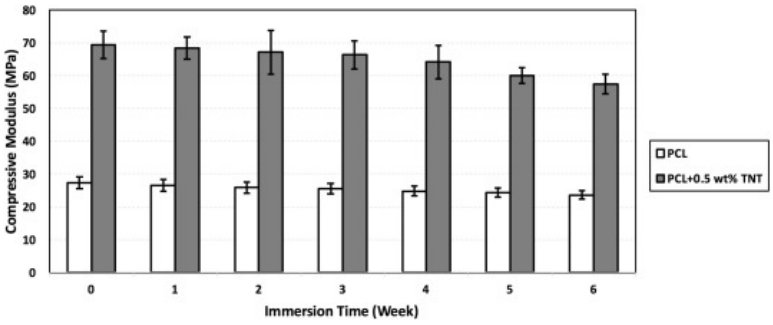

Fig. 8. Compressive modulus of the PCl and PCL/TNT (0.5 wt%) scaffolds over the 6 weeks' degradation period (n = 5).

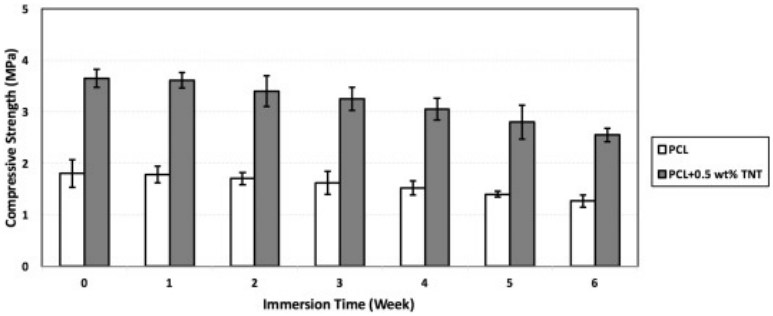

Fig. 9. Compressive strength of the PCl and PCL/TNT (0.5 wt%) scaffolds over the 6 weeks' degradation period (n = 5).

In order to have a better understanding of the effect of fillers (TiO_2 nanotube) and processing conditions on the degradation of the composite, it is essential to review the mechanisms and the factors that could affect the polymer degradation.

Aliphatic polyesters decompose through hydrolytic degradation. When in aqueous media, degradation occurs through cleavage of the ester bond.[85] Although a number of research studies have been carried out on the preparation and degradation of these materials, the role of the low molecular weight fragments in the degradation process is still unknown. Schliecker et al.[86] proposed that the hydrolytic degradation process could be influenced by four parameters: particularly, the rate constant, the amount of water that has been uptaked, the diffusion coefficient of the chain parts, and the solubility of the

Materials Science and Engineering: C, Vol. 70, No. 1 (January 1, 2017): pg. 586-598. DOI. This article is © Elsevier and permission has been granted for this version to appear in e-Publications@Marquette. Elsevier does not grant permission for this article to be further copied/distributed or hosted elsewhere without the express permission from Elsevier.

***NOT THE PUBLISHED VERSION;* this is the author's final, peer-reviewed manuscript.** The published version may be accessed by following the link in the citation at the bottom of the page.

degradation byproducts in the fluid media. The degradation of a polymer matrix could proceed *via* the following mechanisms:

(i)surface or heterogeneous and
(ii)bulk or homogeneous erosion.[86]

In the first case,[1] water is being absorbed by the polymer and hydrolytic ester cleavage occurs at the surface of the polymer matrix. This generates chain fragments that have acidic end groups. At first, polymer degradation is faster than water intrusion into the polymer bulk, which causes degradation primarily in the furthest area and not in the internal part of the matrix. The decrease in molecular weight, along with an increase in the polydispersity, M_w/M_n, and polymer mass loss occur. After a short time, water diffusion is relatively rapid in comparison to polymer degradation. Reaction/diffusion phenomena, which involve water soluble low molecular weight degradation products at the surface and the inner part of the polymer, govern polymer degradation.[85] In small size medical devices, soluble oligomers can escape before the devices are fully degraded. In contrast, in large size devices, only soluble oligomers that are found near to the outer surface can escape, while the ones inside the device remain entrapped as a result of their relatively small diffusion coefficients. Consequently, carboxyl end groups are more concentrated in the center, and the degradation rate increases due to autocatalysis of ester hydrolysis by the carboxyl groups.[85,86]

In the second case of homogeneous erosion, polymers degrade slowly and water diffusion into the system is faster than polymer degradation. Accordingly, the entire system hydrates quickly, and when the polymers change into oligomers, they are separated throughout. It is essential to note that degradable polymers can erode *via* both pathways depending on the erosion conditions, the geometry of the samples, and the hydrophilic/hydrophobic characteristics of the polymer.[86] Initially, the degradation continues through the amorphous sections, since they have higher water uptake ability than the crystalline ones. The degraded parts diffuse and then recrystallize. The degree of crystallinity could increase along with degradation. After the major part of the amorphous area degrades, hydrolysis proceeds from the edge to the center of the crystalline domains.[86]

Polycaprolactone is also a semi-crystalline aliphatic polyester but with higher crystallinity and hydrophobicity than polylactic acid, and as a result, it shows a different degradation behavior. The hydrophobicity of polycaprolactone could be attributed to a surface erosion/degradation characteristic as Xu et al.[87] illustrated in their study of hydrophobic polyesters. Polycaprolactone has lower degradation rates than polylactic acid,

Materials Science and Engineering: C, Vol. 70, No. 1 (January 1, 2017): pg. 586-598. DOI. This article is © Elsevier and permission has been granted for this version to appear in e-Publications@Marquette. Elsevier does not grant permission for this article to be further copied/distributed or hosted elsewhere without the express permission from Elsevier.

***NOT THE PUBLISHED VERSION;* this is the author's final, peer-reviewed manuscript.** The published version may be accessed by following the link in the citation at the bottom of the page.

but being highly compatible with osteoblasts is useful for long-term implant applications.[87,88]

This change in mechanical properties after soaking in SBF is due to two opposite effects.[89] On one hand, the research studies ascertain faster degradation of the amorphous phase of material than the crystalline phase, increasing the crystallinity and thus the mechanical properties. On the other hand, degradation produces mass loss and porosity in the sample, resulting in a decrease of mechanical properties (Young's modulus).[90] The porosity can be produced inside the sample, if bulk degradation takes places, or near the surface of the sample, if superficial erosion is the degradation mechanism.[91]

3.4. *In vitro* biological evaluations

3.4.1. MTT assay

The results given by MTT assay were compared to the control group (polystyrene well) as shown in Fig. 10. According to the results, the addition of TNT to polymeric scaffolds had no negative effect on the proliferation of G-292 cells. Also, viabilities were better for nanocomposite scaffolds [PCL/TNT (0.5 wt%)] using G-292 cell line; however, they resulted in a significant reduction in the biocompatibility of the nanocomposite samples in comparison to the control group only after 3 days' incubation time. With increasing incubation periods (14 days), viabilities improved even comparing with the control group [112.5 $\pm$ 5.2% for PCL/TNT (0.5 wt%) and 95 $\pm$ 7.5% for pure PCL scaffold] (p value < 0.05).

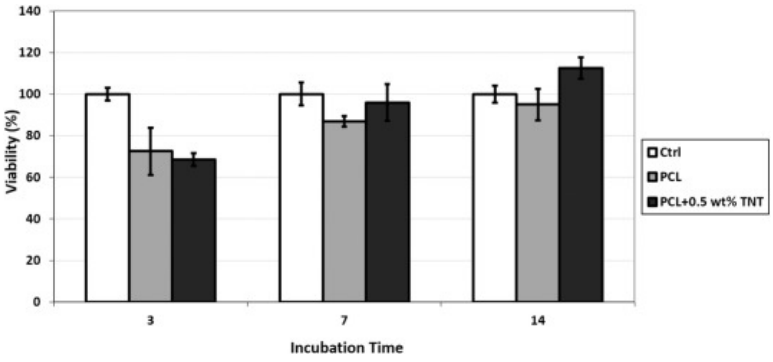

Fig. 10. Cell proliferation of G-292 cells proliferated on the PCL/TNT (0.5 wt%) scaffolds along with negative control after incubation for 3, 7, and 14 days (n = 5).

Materials Science and Engineering: C, Vol. 70, No. 1 (January 1, 2017): pg. 586-598. DOI. This article is © Elsevier and permission has been granted for this version to appear in e-Publications@Marquette. Elsevier does not grant permission for this article to be further copied/distributed or hosted elsewhere without the express permission from Elsevier.

***NOT THE PUBLISHED VERSION;* this is the author's final, peer-reviewed manuscript.** The published version may be accessed by following the link in the citation at the bottom of the page.

3.4.2. ALP activity

ALP is a well-known analysis for the differentiation of osteoblasts during osteogenesis. ALP activity results for G-292 cells on the PCL and PCL/TNT (0.5 wt%) scaffold is given for 3, 7, and 14 days of incubation period (see Fig. 11). The obtained results confirmed that there is a general trend of increasing in ALP activity for PCL/TNT (0.5 wt%) scaffold by time (117.4 $\pm$ 7.4% for 14 days and 87.6 $\pm$ 4.4% for 1 day) (p value < 0.05).

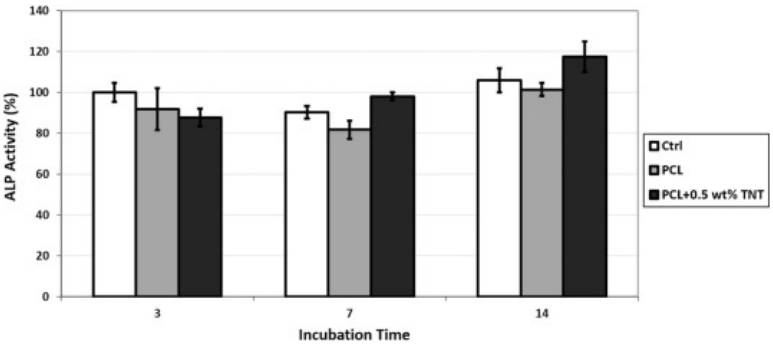

Fig. 11. ALP activity test for G-292 cells proliferated on the PCL/TNT (0.5 wt%) scaffolds along with negative control after incubation for 3, 7, and 14 days (n = 5).

3.4.3. SEM observations of cell morphology

In the current study, the cytocompatibility tests of the PCL/TNT (0.5 wt%) scaffold was carried out using SaOS-2 cells, a human osteoblast-like cell line. SEM micrographs of SaOS-2 cells cultured on the surface of the scaffold is presented as Fig. 12. After 7 days of culture, SaOS-2 cells spread well over the surface and showed normal morphology and phenotype. Also, the connection of the cells to each other can be observed in this figure. The cells displayed filopodia anchorage and proliferated well on the surface of the scaffold. The cells on the surface of the prepared scaffold appeared to be elongated as well as well attached and spread. It is noticeable that the cells were anchored to the surface of the scaffold by discrete filopodia. It was also revealed that the cells are penetrating into the scaffolds through their pores.

Materials Science and Engineering: C, Vol. 70, No. 1 (January 1, 2017): pg. 586-598. DOI. This article is © Elsevier and permission has been granted for this version to appear in e-Publications@Marquette. Elsevier does not grant permission for this article to be further copied/distributed or hosted elsewhere without the express permission from Elsevier.

***NOT THE PUBLISHED VERSION;* this is the author's final, peer-reviewed manuscript.** The published version may be accessed by following the link in the citation at the bottom of the page.

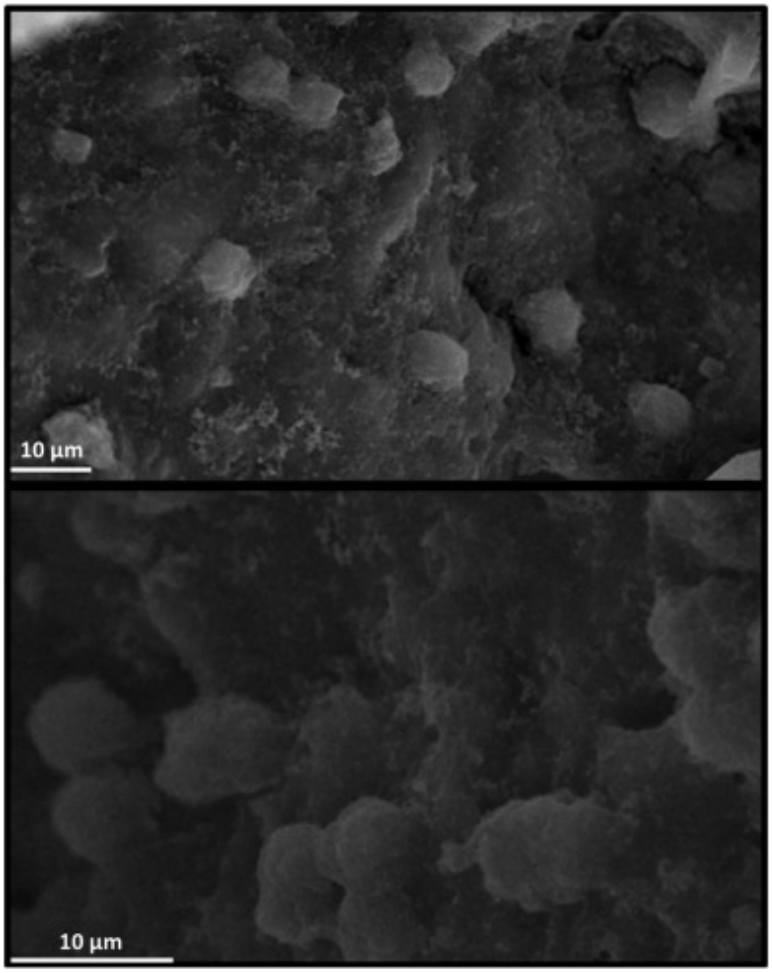

Fig. 12. Morphology of SaOS-2 cells cultured on the PCL/TNT (0.5 wt%) scaffold at different magnifications.

3.4.4. RT-PCR analysis

A quantitative RT-PCR method was employed to determine gene expression of osteoblasts after 3 and 7 days. In order to know whether MC3T3-E1 pre-osteoblast differentiation was affected by PCL/TNT (0.5 wt%), we chose COL-1, OCN, and RUNX-2 as markers for osteoblastic differentiation in this paper. Among bone matrices, COL-1 is the most abundant protein synthesized by active osteoblasts and conductive to mineral deposition. Osteocalcin is chosen solely by osteoblasts and thought to play an important role in the body's metabolic regulation, and it is pro-osteoblastic, or bone-building.[92] It is additionally involved in bone mineralization and calcium ion homeostasis. RUNX-2 gene is a member of the RUNX family of transcription factors and encodes a nuclear protein with a runt DNA-binding domain. The protein could bind DNA both as a monomer and, with more

Materials Science and Engineering: C, Vol. 70, No. 1 (January 1, 2017): pg. 586-598. DOI. This article is © Elsevier and permission has been granted for this version to appear in e-Publications@Marquette. Elsevier does not grant permission for this article to be further copied/distributed or hosted elsewhere without the express permission from Elsevier.

***NOT THE PUBLISHED VERSION;* this is the author's final, peer-reviewed manuscript.** The published version may be accessed by following the link in the citation at the bottom of the page.

affinity, as a subunit of a heterodimeric complex. This protein has been considered a key transcription factor associated with osteoblast differentiation.[93] The obtained RT-PCR results for mRNA expression of osteocalcin and RUNX-2, both of which are osteoblast markers, are revealed as fold enhances.

As it can be seen in the Fig. 13, there are significant differences in the osteocalcin expression between PCL/TNT (0.5 wt%) and PCL at day 3 (and 7 (p value < 0.05) (see Fig. 13(a)). The osteocalcin expression was 1.26-fold higher on day 3 and about 5-fold higher on day 7 for the PCL/TNT (0.5 wt%) as opposed to the PCL samples. Also, the RUNX-2 expression was significantly higher by day 7 for the PCL/TNT (0.5 wt%) as opposed to the PCL samples (see Fig. 13(b). The COL-1 expression was significantly lower by day 3 for the PCL/TNT (0.5 wt%) as opposed to the PCL samples. However, significant higher COL-1 expression of PCL/TNT (0.5 wt%) than PCL samples was seen at day 7 (p value < 0 0.05) (see Fig. 13(c).

Materials Science and Engineering: C, Vol. 70, No. 1 (January 1, 2017): pg. 586-598. DOI. This article is © Elsevier and permission has been granted for this version to appear in e-Publications@Marquette. Elsevier does not grant permission for this article to be further copied/distributed or hosted elsewhere without the express permission from Elsevier.

***NOT THE PUBLISHED VERSION;* this is the author's final, peer-reviewed manuscript.** The published version may be accessed by following the link in the citation at the bottom of the page.

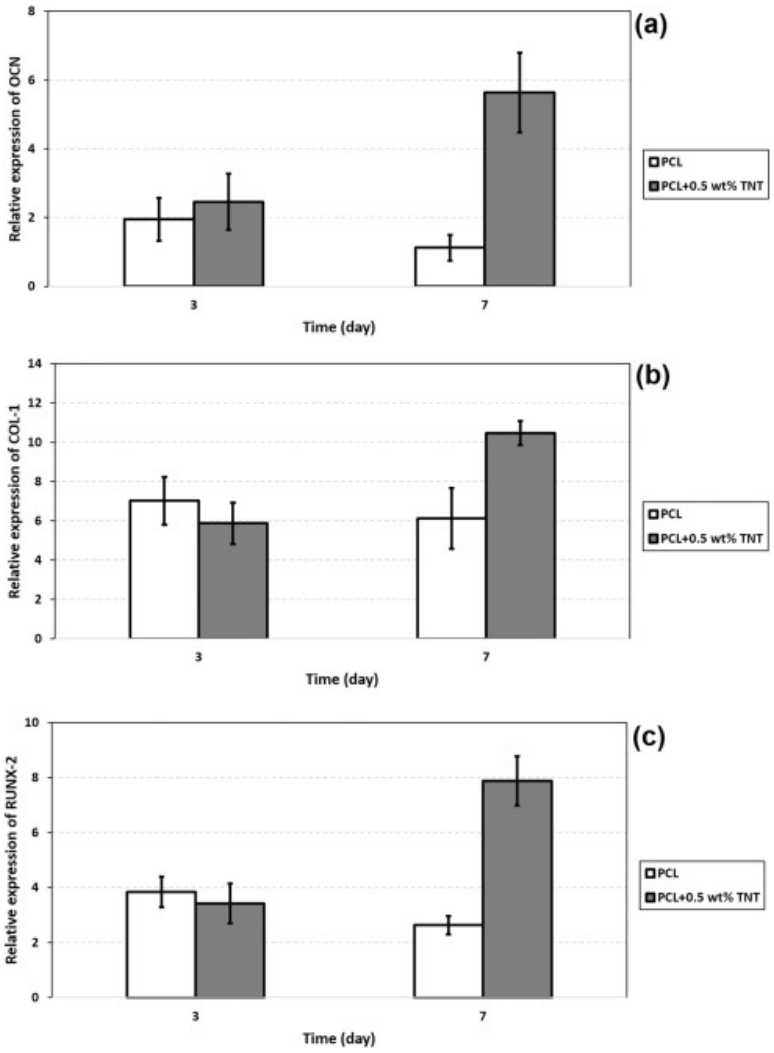

Fig. 13. Quantitative real-time PCR analysis for (a) OCN, (b) RUNX-2 and (c) COL-1 on the PCL and PCL/TNT (0.5 wt%) scaffold as a function of incubation time (n = 5).

According to the obtained results, better osteoblast viability and differentiation marked by higher OCN, RUNX-2 and COL-1 expression were seen on PCL/TNT (0.5 wt%) rather than PCL surfaces. The addition of TiO_2 nanotube to the PCL caused significantly increased osteoblast differentiation. There are several factors that could attribute to increased mineralized matrix production when osteoblasts were cultured on PCL/TNT (0.5 wt%) scaffolds. Finally, the obtained gene expression results provide evidence that the prepared scaffold constitutes a good substrate for MC3T3-E1 cell differentiation prompting ECM mineralization.

Materials Science and Engineering: C, Vol. 70, No. 1 (January 1, 2017): pg. 586-598. DOI. This article is © Elsevier and permission has been granted for this version to appear in e-Publications@Marquette. Elsevier does not grant permission for this article to be further copied/distributed or hosted elsewhere without the express permission from Elsevier.

***NOT THE PUBLISHED VERSION;* this is the author's final, peer-reviewed manuscript.** The published version may be accessed by following the link in the citation at the bottom of the page.

4. Conclusions

In conclusion, we fabricated 3D scaffolds based on the microsphere sintering method in this paper. This technique provides a quick, reproducible, mild and flexible means for creating a 3D scaffold and permits the independent control over pore size, interconnection and mechanical properties. It was demonstrated that the sintered scaffold had an interconnected porous structure, and the mechanical properties were suitable for load-bearing bone tissue engineering applications. The obtained experimental results confirmed that PCL/TNT (0.5 wt%) exhibited higher compressive modulus and compressive strength compared to other prepared scaffolds, and thus, this scaffold was selected as an ideal one for further investigation of mechanical characteristics. In fact, loadings beyond 0.5 wt% TNT in the starting material led to a reduction in the mechanical properties of these prepared scaffolds, due in part to the aggregation of nanotubes. Moreover, the increase in compressive modulus and compressive strength at smaller microsphere diameters could be attributed to the decrease in total porosity of the scaffolds. Moreover, the *in vitro* biological properties data revealed that the PCL/TNT (0.5 wt%) had a better biocompatibility and bioactivity than PCL scaffolds. Also, the obtained results from quantitative RT-PCR provide evidence that the PCL scaffold containing TiO_2 nanotube constitutes an excellent substrate for cell differentiation, leading to ECM mineralization. Eventually, the future work will be focused on complex tissue replacement by micropositioning the building blocks of the scaffold in order to exhibit complex arrays of biophysical and biochemical signals following a tight dose, time and space control.

References

[1]L.G. Griffith, G. Naughton **Tissue engineering–current challenges and expanding opportunities** *Science*, 295 (5557) (2002), pp. 1009-1014

[2]R. Ravarian, F. Moztarzadeh, M.S. Hashjin, S. Rabiee, P. Khoshakhlagh, M. Tahriri **Synthesis, characterization and bioactivity investigation of bioglass/hydroxyapatite composite** *Ceram. Int.,* 36 (1) (2010), pp. 291-297

[3]M. Mozafari, F. Moztarzadeh, M. Rabiee, M. Azami, S. Maleknia, M. Tahriri, *et al.* **Development of macroporous nanocomposite scaffolds of gelatin/bioactive glass prepared through layer solvent casting combined with lamination technique for bone tissue engineering** *Ceram. Int.,* 36 (8) (2010), pp. 2431-2439

[4]H. Nojehdehian, F. Moztarzadeh, H. Baharvand, H. Nazarian, M. Tahriri **Preparation and surface characterization of poly-l-lysine-coated PLGA microsphere scaffolds containing retinoic acid for nerve tissue engineering: in vitro study** *Colloids Surf. B: Biointerfaces*, 73 (1) (2009), pp. 23-29

Materials Science and Engineering: C, Vol. 70, No. 1 (January 1, 2017): pg. 586-598. DOI. This article is © Elsevier and permission has been granted for this version to appear in e-Publications@Marquette. Elsevier does not grant permission for this article to be further copied/distributed or hosted elsewhere without the express permission from Elsevier.

***NOT THE PUBLISHED VERSION;* this is the author's final, peer-reviewed manuscript.** The published version may be accessed by following the link in the citation at the bottom of the page.

[5]M. Azami, F. Moztarzadeh, M. Tahriri **Preparation, characterization and mechanical properties of controlled porous gelatin/hydroxyapatite nanocomposite through layer solvent casting combined with freeze-drying and lamination techniques** *J. Porous. Mater.*, 17 (3) (2010), pp. 313-320

[6]M. Kabiri, S.H. Emami, M. Rafinia, M. Tahriri **Preparation and characterization of absorbable hemostat crosslinked gelatin sponges for surgical applications** *Curr. Appl. Phys.*, 11 (3) (2011), pp. 457-461

[7]H. Nojehdehian, F. Moztarzadeh, H. Baharvand, N.Z. Mehrjerdi, H. Nazarian, M. Tahriri **Effect of poly-l-lysine coating on retinoic acid-loaded PLGA microspheres in the differentiation of carcinoma stem cells into neural cells** *The International journal of artificial organs.*, 33 (10) (2010), pp. 721-730

[8]M. Mozafari, F. Moztarzadeh, M. Rabiee, M. Azami, N. Nezafati, Z. Moztarzadeh, *et al.* **Development of 3 D bioactive nanocomposite scaffolds made from gelatin and NANO bioactive glass for biomedical applications** *Adv. Compos. Lett.*, 19 (2) (2010), pp. 91-96

[9]M. Ashuri, F. Moztarzadeh, N. Nezafati, A.A. Hamedani, M. Tahriri **Development of a composite based on hydroxyapatite and magnesium and zinc-containing sol–gel-derived bioactive glass for bone substitute applications** *Mater. Sci. Eng. C,* 32 (8) (2012), pp. 2330-2339

[10]S. Poursamar, M. Rabiee, A. Samadikuchaksaraei, M. Tahriri, M. Karimi, M. Azami **Influence of the value of the pH on the preparation of nano hydroxyapatite polyvinyl alcohol composites** *J Ceram Process Res.*, 10 (5) (2009), pp. 679-682

[11]M. Tahriri, F. Moztarzadeh **Preparation, characterization, and in vitro biological evaluation of PLGA/nano-fluorohydroxyapatite (FHA) microsphere-sintered scaffolds for biomedical applications** *Appl. Biochem. Biotechnol.*, 172 (5) (2014), pp. 2465-2479

[12]S. Ayati Najafabadi, H. Keshvari, Y. Ganji, M. Tahriri, M. Ashuri **Chitosan/heparin surface modified polyacrylic acid grafted polyurethane film by two step plasma treatment** *Surf. Eng.*, 28 (9) (2012), pp. 710-714

[13]D. Bizari, F. Moztarzadeh, M. Rabiee, M. Tahriri, F. Banafatizadeh, A. Ansari, *et al.* **Development of biphasic hydroxyapatite/dicalcium phosphate dihydrate (DCPD) bone graft using polyurethane foam template: in vitro and in vivo study** *Adv. Appl. Ceram.*, 110 (7) (2011), pp. 417-425

[14]M. Raz, F. Moztarzadeh, M.A. Shokrgozar, M. Azami, M. Tahriri **Development of biomimetic gelatin–chitosan/hydroxyapatite nanocomposite via double diffusion method for biomedical applications** *Int. J. Mater. Res.*, 105 (5) (2014), pp. 493-501

[15]T. Hooshmand, A. Abrishamchian, F. Najafi, M. Mohammadi, H. Najafi, M. Tahriri **Development of sol-gel-derived multi-wall carbon nanotube/hydroxyapatite nanocomposite powders for bone substitution** *J. Compos. Mater.*, 0021998313475368 (2013)

[16]Y. Zamani, M. Rabiee, M.A. Shokrgozar, S. Bonakdar, M. Tahriri **Response of human mesenchymal stem cells to patterned and randomly oriented poly (vinyl alcohol) nano-fibrous scaffolds surface-modified with Arg-Gly-asp (RGD) ligand** *Appl. Biochem. Biotechnol.*, 171 (6) (2013), pp. 1513-1524

[17]M. Haghbin-Nazarpak, F. Moztarzadeh, M. Solati-Hashjin, A.R. Mirhabibi, M. Tahriri **Preparation, characterization and gentamicin sulfate release investigation of biphasic injectable calcium phosphate bone cement** *Ceramics-Silikáty*, 54 (2010), pp. 334-340

[18]R. Masaeli, J. Kashi, T. Sadat, R. Dinarvand, M. Tahriri, V. Rakhshan, *et al.* **Preparation, characterization and evaluation of drug release properties of simvastatin-loaded PLGA microspheres** *Iranian Journal of Pharmaceutical Research.*, 15 (2016), pp. 205-211

Materials Science and Engineering: C, Vol. 70, No. 1 (January 1, 2017): pg. 586-598. DOI. This article is © Elsevier and permission has been granted for this version to appear in e-Publications@Marquette. Elsevier does not grant permission for this article to be further copied/distributed or hosted elsewhere without the express permission from Elsevier.

***NOT THE PUBLISHED VERSION;* this is the author's final, peer-reviewed manuscript.** The published version may be accessed by following the link in the citation at the bottom of the page.

[19]R. Masaeli, T.S. Jafarzadeh Kashi, R. Dinarvand, M. Tahriri, H. Shahoon, M. Raz, *et al.* **Preparation, characterization and investigation of in vitro and in vivo biological properties of strontium-modified calcium phosphate cement for bone defect repair** *Journal of Dental Medicine.*, 28 (3) (2015), pp. 177-188

[20]S. Naghavi Alhosseini, F. Moztarzadeh, S. Kargozar, M. Dodel, M. Tahriri **Development of polyvinyl alcohol fibrous biodegradable scaffolds for nerve tissue engineering applications: in vitro study** *International Journal of Polymeric Materials and Polymeric Biomaterials.*, 64 (9) (2015), pp. 474-480

[21]J. Liu, L. Reni, Q. Wei, J. Wu, S. Liu, Y. Wang, *et al.* **Fabrication and characterization of polycaprolactone/calcium sulfate whisker composites** *Express Polym Lett*, 5 (8) (2011), pp. 742-752

[22]G.J. Nohynek, J. Lademann, C. Ribaud, M.S. Roberts **Grey goo on the skin? Nanotechnology, cosmetic and sunscreen safety** *Crit. Rev. Toxicol.*, 37 (3) (2007), pp. 251-277

[23]H. Liu, E.B. Slamovich, T.J. Webster **Increased osteoblast functions on nanophase titania dispersed in poly-lactic-*co*-glycolic acid composites** *Nanotechnology*, 16 (7) (2005), p. S601

[24]K. Goto, J. Tamura, S. Shinzato, S. Fujibayashi, M. Hashimoto, M. Kawashita, *et al.* **Bioactive bone cements containing nano-sized titania particles for use as bone substitutes** *Biomaterials*, 26 (33) (2005), pp. 6496-6505

[25]H. Eslami, M. Solati-Hashjin, M. Tahriri **The comparison of powder characteristics and physicochemical, mechanical and biological properties between nanostructure ceramics of hydroxyapatite and fluoridated hydroxyapatite** *Mater. Sci. Eng. C,* 29 (4) (2009), pp. 1387-1398

[26]H. Eslami, M. Solati-Hashjin, M. Tahriri **Synthesis and characterization of nanocrystalline fluorinated hydroxyapatite powder by modified wet-chemical process** *J Ceram Process Res.*, 9 (2008), pp. 224-229

[27]E. Shafia, M. Bodaghi, M. Tahriri **The influence of some processing conditions on host crystal structure and phosphorescence properties of SrAl 2 O 4: Eu 2 +, Dy 3 + nanoparticle pigments synthesized by combustion technique** *Curr. Appl. Phys.*, 10 (2) (2010), pp. 596-600

[28]M. Bodaghi, A. Mirhabibi, H. Zolfonun, M. Tahriri, M. Karimi **Investigation of phase transition of γ-alumina to α-alumina via mechanical milling method** *Phase Transit.*, 81 (6) (2008), pp. 571-580

[29]F. Kazemi, A. Saberi, S. Malek-Ahmadi, S. Sohrabi, H. Rezaie, T. M. **Novel method for synthesis of metastable tetragonal zirconia nanopowders at low temperatures** *Ceramics-Silikáty*, 55 (1) (2011), pp. 26-30

[30]M. Karimi, M. Rabiee, F. Moztarzadeh, M. Bodaghi, M. Tahriri **Ammonia-free method for synthesis of CdS nanocrystalline thin films through chemical bath deposition technique** *Solid State Commun.*, 149 (41) (2009), pp. 1765-1768

[31]H. Eslami, M. Tahriri, F. Bakhshi **Synthesis and characterization of nanocrystalline hydroxyapatite obtained by the wet chemical technique** *Materials Science-Poland.*, 28 (1) (2010), pp. 5-13

[32]A. Zamanian, F. Moztarzadeh, S. Kordestani, S. Hesaraki, M. Tahriri **Novel calcium hydroxide/nanohydroxyapatite composites for dental applications: in vitro study** *Adv. Appl. Ceram.*, 109 (7) (2010), pp. 440-444

[33]M. Mozafari, F. Moztarzadeh, M. Tahriri **Green synthesis and characterisation of spherical PbS luminescent micro-and nanoparticles via wet chemical technique** *Adv. Appl. Ceram.*, 110 (1) (2011), pp. 30-34

Materials Science and Engineering: C, Vol. 70, No. 1 (January 1, 2017): pg. 586-598. DOI. This article is © Elsevier and permission has been granted for this version to appear in e-Publications@Marquette. Elsevier does not grant permission for this article to be further copied/distributed or hosted elsewhere without the express permission from Elsevier.

***NOT THE PUBLISHED VERSION;* this is the author's final, peer-reviewed manuscript.** The published version may be accessed by following the link in the citation at the bottom of the page.

[34]E. Mohagheghpour, M. Rabiee, F. Moztarzadeh, M. Tahriri, M. Jafarbeglou, D. Bizari, *et al.* **Controllable synthesis, characterization and optical properties of ZnS: Mn nanoparticles as a novel biosensor** *Mater. Sci. Eng. C,* 29 (6) (2009), pp. 1842-1848

[35]H. Sameie, R. Salimi, A.S. Alvani, A. Sarabi, F. Moztarzadeh, M. Tahriri **Evaluation of sol–gel derived Eu 2 + activated SrMgAl 2 SiO 7 as a novel nanostructure luminescent pigment** *Phys. B Condens. Matter*, 405 (23) (2010), pp. 4796-4800

[36]M. Bodaghi, A. Mirhabibi, M. Tahriri, H. Zolfonoon, M. Karimi **Mechanochemical assisted synthesis and powder characteristics of nanostructure ceramic of α-Al 2 O 3 at room temperature** *Mater. Sci. Eng. B*, 162 (3) (2009), pp. 155-161

[37]M. Bodaghi, H. Zolfonoon, M. Tahriri, M. Karimi **Synthesis and characterization of nanocrystalline α-Al 2 O 3 using Al and Fe 2 O 3 (hematite) through mechanical alloying** *Solid State Sci.*, 11 (2) (2009), pp. 496-500

[38]M.E. Khosroshahi, L. Ghazanfari, M. Tahriri **Characterisation of binary (Fe3O4/SiO2) biocompatible nanocomposites as magnetic fluid** *J. Exp. Nanosci.*, 6 (6) (2011), pp. 580-595

[39]R. Salimi, H. Sameie, A.S. Alvani, A. Sarabi, H.E. Mohammadloo, F. Nargesian, *et al.* **SrZn 2 Si 2 O 7: Eu 2 +, Mn 2 +: a single-phased emission tunable nanophosphor suitable for white light emitting diodes** *JOSA B.*, 30 (6) (2013), pp. 1747-1754

[40]R. Salimi, H. Sameie, A. Sabbagh Alvani, A. Sarabi, F. Moztarzadeh, M. Tahriri **Sol–gel synthesis, characterization and luminescence properties of SrMgAl2SiO7: Eu2 + as a novel nanocrystalline phosphor** *Luminescence*, 26 (6) (2011), pp. 449-455

[41]E. Shafia, A. Aghaei, A. Davarpanah, M. Bodaghi, M. Tahriri, S. Alavi **Synthesis and characterization of SrAl2O4: Eu2 +, Dy3 + nanocrystalline phosphorescent pigments** *Transactions of the Indian Ceramic Society.*, 70 (2) (2011), pp. 71-77

[42]M. Bodaghi, A. Mirhabibi, H. Zolfonoon, M. Salehie, M. Tahriri **Preparation and characterisation of α-Al2O3 powder from γ-Al2O3 powder using mechanical milling technique** *Mater. Res. Innov.*, 12 (4) (2008), pp. 157-161

[43]R. Salimi, H. Sameie, A.S. Alvani, A. Sarabi, F. Moztarzadeh, H.E. Mohammadloo, *et al.* **Sol–gel synthesis, structural and optical characteristics of Sr1 − x Zn2Si2yO7 + δ: xEu2 + as a potential nanocrystalline phosphor for near-ultraviolet white light-emitting diodes** *J. Mater. Sci.*, 47 (6) (2012), pp. 2658-2664

[44]E. Mohagheghpour, F. Moztarzadeh, M. Rabiee, M. Tahriri, M. Ashuri, H. Sameie, *et al.* **Micro-emulsion synthesis, surface modification, and Photophysical properties of nanocrystals for biomolecular recognition** *NanoBioscience, IEEE Transactions on.*, 11 (4) (2012), pp. 317-323

[45]E. Shafia, A. Aghaei, M. Bodaghi, M. Tahriri **Combusion synthesis, structural and photo-physical characteristics of Eu2 + and Dy3 + co-doped SrAl2O4 phosphor nanopowders** *J. Mater. Sci. Mater. Electron.*, 22 (8) (2011), pp. 1136-1142

[46]F.S. Jazi, N. Parvin, M. Rabiei, M. Tahriri, Z.M. Shabestari, A.R. Azadmehr **Effect of the synthesis route on the grain size and morphology of ZnO/Ag nanocomposite** *Journal of Ceramic Processing Research.*, 13 (5) (2012), pp. 523-526

[47]F. Shafiei, M. Behroozibakhsh, F. Moztarzadeh, M. Haghbin-Nazarpak, M. Tahriri **Nanocrystalline fluorine-substituted hydroxyapatite [Ca 5 (PO 4) 3 (OH) 1-x F × (0 ⩽ x ⩽ 1)] for biomedical applications: preparation and characterization** *Micro & Nano Letters, IET.*, 7 (2) (2012), pp. 109-114

Materials Science and Engineering: C, Vol. 70, No. 1 (January 1, 2017): pg. 586-598. DOI. This article is © Elsevier and permission has been granted for this version to appear in e-Publications@Marquette. Elsevier does not grant permission for this article to be further copied/distributed or hosted elsewhere without the express permission from Elsevier.

***NOT THE PUBLISHED VERSION;* this is the author's final, peer-reviewed manuscript.** The published version may be accessed by following the link in the citation at the bottom of the page.

[48]D. Bizari, M. Rabiee, F. Moztarzadeh, M. Tahriri, S. Alavi, R. Masaeli **Synthesis, characterization and biological evaluation of sol–gel derived nanomaterial in the ternary system 64% SiO2-31% CaO-5% P2O5 as a bioactive glass: in vitro study** *Ceramics-Silikáty*, 57 (3) (2013), pp. 201-209

[49]E. Mohagheghpour, M. Rabiee, F. Moztarzadeh, M. Tahriri **Effect of manganese (Mn) doping on the optical properties of zinc sulfide (ZnS) semiconductor nanocrystals** *J Ceram Process Res.*, 11 (2010), pp. 144-149

[50]S. Solgi, M. Khakbiz, M. Shahrezaee, A. Zamanian, M. Tahriri, S. Keshtkari, *et al.* **Synthesis, characterization and in vitro biological evaluation of Sol-gel derived Sr-containing Nano bioactive glass** *SILICON*, 1-8 (2015)

[51]F.S. Jazi, N. Parvin, M. Tahriri, M. Alizadeh, S. Abedini, M. Alizadeh **The relationship between the synthesis and morphology of SnO2-Ag2O nanocomposite** *Synthesis and Reactivity in Inorganic, Metal-Organic, and Nano-Metal Chemistry.*, 44 (5) (2014), pp. 759-764

[52]R. Salimi, H. Sameie, A.S. Alvani, A. Sarabi, M. Khorasani, M.M. Farsi, *et al.* **Optical characterization of the novel nanostructure Eudoped phosphor for potential application in LEDs** *Conference on Lasers and Electro-Optics/Pacific Rim, Optical Society of America* (2011)

[53]H. Sameie, R. Salimi, A.S. Alvani, A. Sarabi, F. Moztarzadeh, M.M. Farsi, *et al.* **A nanostructure phosphor: effect of process parameters on the photoluminescence properties for near-UV WLED applications** *J. Inorg. Organomet. Polym. Mater.*, 22 (4) (2012), pp. 737-743

[54]M. Raz, F. Moztarzadeh, A.A. Hamedani, M. Ashuri, M. Tahriri **Controlled synthesis, characterization and magnetic properties of magnetite (Fe3O4) nanoparticles without surfactant under N2 gas at room temperature** *Key Eng. Mater.* (2012)

[55]H. Eslami, F. Moztarzadeh, M. Tahriri **Synthesis, characterisation and thermal properties of Ca5 (PO4) 3 (OH) 1 − xFx (0 ⩽ x ⩽ 1) nanopowders via pH cycling method** *Mater. Res. Innov.*, 15 (3) (2011), pp. 190-195

[56]E. Mohagheghpour, R. Salimi, H. Sameie, F. Moztarzadeh, M. Roohnikan, M.A.M. Farsi, *et al.* **A new optical bio-sensor: Wet-chemical synthesis and surface treatment of nanocrystalline Zn 1-x S: Mn + 2 x. Optical Sensors** *Optical Society of America* (2011)

[57]H. Eslami FM, T.S.J. Kashi, K. Khoshroo, M. Tahriri **Hydrothermal Synthesis and Characterization of TiO2-Derived Nanotubes for Biomedical Applications** *Synthesis and Reactivity in Inorganic, Metal-Organic, and Nano-Metal Chemistry,* 46 (8) (2016), pp. 1149-1156

[58]K. Khoshroo TSJK, F. Moztarzadeh, H. Eslami, M. Tahriri **The influence of calcination temperature on the structural and biological characteristics of hydrothermally synthesized TiO2 nanotube: in vitro study** *Synthesis and Reactivity in Inorganic, Metal-Organic, and Nano-Metal Chemistry*, 46 (8) (2016), pp. 1189-1194

[59]M. Borden, M. Attawia, Y. Khan, C.T. Laurencin **Tissue engineered microsphere-based matrices for bone repair: design and evaluation** *Biomaterials*, 23 (2) (2002), pp. 551-559

[60]K. Khoshroo Jafarzadeh kashi TS, Moztarzadeh F, Eslami H, Tahriri M. **The influence of calcination temperature on the structural and biological characteristics of hydrothermally synthesized TiO2 nanotube: in vitro study** *Synthesis and Reactivity in Inorganic, Metal-Organic, and Nano-Metal Chemistry.*, 46 (8) (2016), pp. 1189-1194

[61]H. Eslami, F. Moztarzadeh, T.S.J. Kashi, K. Khoshroo, M. Tahriri **Hydrothermal synthesis and characterization of TiO2-derived nanotubes for biomedical applications** *Synthesis and Reactivity in Inorganic, Metal-Organic, and Nano-Metal Chemistry.*, 46 (8) (2016), pp. 1149-1156

Materials Science and Engineering: C, Vol. 70, No. 1 (January 1, 2017): pg. 586-598. DOI. This article is © Elsevier and permission has been granted for this version to appear in e-Publications@Marquette. Elsevier does not grant permission for this article to be further copied/distributed or hosted elsewhere without the express permission from Elsevier.

***NOT THE PUBLISHED VERSION;* this is the author's final, peer-reviewed manuscript.** The published version may be accessed by following the link in the citation at the bottom of the page.

[62]L.M. Nikolić, M. Maletin, P. Ferreira, P.M. Vilarinho **Synthesis and characterization of one-dimensional titanate structure** *Process Appl Ceram.*, 2 (2008), pp. 109-114

[63]M. Qamar, C. Yoon, H. Oh, N. Lee, K. Park, D. Kim, *et al.* **Preparation and photocatalytic activity of nanotubes obtained from titanium dioxide** *Catal. Today*, 131 (1) (2008), pp. 3-14

[64]A. Luciani, V. Guarino, L. Ambrosio, P. Netti **Solvent and melting induced microspheres sintering techniques: a comparative study of morphology and mechanical properties** *J. Mater. Sci. Mater. Med.*, 22 (9) (2011), pp. 2019-2028

[65]C. Durucan, P.W. Brown **Low temperature formation of calcium-deficient hydroxyapatite-PLA/PLGA composites** *J. Biomed. Mater. Res.*, 51 (4) (2000), pp. 717-725

[66]T. Jiang, W.I. Abdel-Fattah, C.T. Laurencin **In vitro evaluation of chitosan/poly (lactic acid-glycolic acid) sintered microsphere scaffolds for bone tissue engineering** *Biomaterials*, 27 (28) (2006), pp. 4894-4903

[67]R.T. Chiroff, R.A. White, E. White, J. Weber, D. Roy **The restoration of articular surfaces overlying replamineform porous biomaterials** *J. Biomed. Mater. Res.*, 11 (2) (1977), pp. 165-178

[68]M. Borden, S. El-Amin, M. Attawia, C. Laurencin **Structural and human cellular assessment of a novel microsphere-based tissue engineered scaffold for bone repair** *Biomaterials*, 24 (4) (2003), pp. 597-609

[69]F. GerVaSO, A. Sannino, G.M. Peretti **The biomaterialist's task: scaffold biomaterials and fabrication technologies** *Joints.*, 1 (3) (2013), p. 130

[70]Q. Lv *Bioreactor-based bone tissue engineering using poly (lactic-co-glycolic acid)/nano-hydroxyapatite composite scaffolds and bone marrow mesenchymal stem cells* (2009)

[71]J.K. Perron, H.E. Naguib, J. Daka, A. Chawla, R. Wilkins **A study on the effect of degradation media on the physical and mechanical properties of porous PLGA 85/15 scaffolds** *J. Biomed. Mater. Res. B Appl. Biomater.*, 91 (2) (2009), pp. 876-886

[72]L. Guan, J.E. Davies **Preparation and characterization of a highly macroporous biodegradable composite tissue engineering scaffold** *J. Biomed. Mater. Res. A*, 71 (3) (2004), pp. 480-487

[73]S. Hulbert, F. Young, R. Mathews, J. Klawitter, C. Talbert, F. Stelling **Potential of ceramic materials as permanently implantable skeletal prostheses** *J. Biomed. Mater. Res.*, 4 (3) (1970), pp. 433-456

[74]F.M. Klenke, Y. Liu, H. Yuan, E.B. Hunziker, K.A. Siebenrock, W. Hofstetter **Impact of pore size on the vascularization and osseointegration of ceramic bone substitutes in vivo** *J. Biomed. Mater. Res. A*, 85 (3) (2008), pp. 777-786

[75]H. Götz, M. Müller, A. Emmel, U. Holzwarth, R. Erben, R. Stangl **Effect of surface finish on the osseointegration of laser-treated titanium alloy implants** *Biomaterials*, 25 (18) (2004), pp. 4057-4064

[76]R. Li, K. Nie, W. Pang, Q. Zhu **Morphology and properties of organic–inorganic hybrid materials involving TiO2 and poly (ϵ-caprolactone), a biodegradable aliphatic polyester** *J. Biomed. Mater. Res. A*, 83 (1) (2007), pp. 114-122

[77]J.A. Goebel, A. Jacob **Use of Mimix hydroxyapatite bone cement for difficult ossicular reconstruction** *Otolaryngol. Head Neck Surg.*, 132 (5) (2005), pp. 727-734

[78]M. Nagano, T. Nakamura, T. Kokubo, M. Tanahashi, M. Ogawa **Differences of bone bonding ability and degradation behaviour in vivo between amorphous calcium phosphate and highly crystalline hydroxyapatite coating** *Biomaterials*, 17 (18) (1996), pp. 1771-1777

Materials Science and Engineering: C, Vol. 70, No. 1 (January 1, 2017): pg. 586-598. DOI. This article is © Elsevier and permission has been granted for this version to appear in e-Publications@Marquette. Elsevier does not grant permission for this article to be further copied/distributed or hosted elsewhere without the express permission from Elsevier.

***NOT THE PUBLISHED VERSION;* this is the author's final, peer-reviewed manuscript.** The published version may be accessed by following the link in the citation at the bottom of the page.

[79]T. Albrektsson, C. Johansson **Osteoinduction, osteoconduction and osseointegration** *Eur. Spine J.,* 10 (2) (2001), pp. S96-S101

[80]R. Johnson, D. Harrison, M. Tucci, A. Tsao, M. Lemos, A. Puckett, *et al.* **Fibrous capsule formation in response to ultrahigh molecular weight polyethylene treated with peptides that influence adhesion** *Biomed. Sci. Instrum.*, 34 (1996), pp. 47-52

[81]T.J. Webster **Nanophase ceramics: the future orthopedic and dental implant material** *Adv. Chem. Eng.*, 27 (2001), pp. 125-166

[82]I. Gotman **Characteristics of metals used in implants** *J. Endourol.*, 11 (6) (1997), pp. 383-389

[83]C.L. Nelson, A.C. McLaren, S.G. McLaren, J.W. Johnson, M.S. Smeltzer **Is aseptic loosening truly aseptic?** *Clin. Orthop. Relat. Res.*, 437 (2005), pp. 25-30

[84]H.-M. Kim, T. Himeno, T. Kokubo, T. Nakamura **Process and kinetics of bonelike apatite formation on sintered hydroxyapatite in a simulated body fluid** *Biomaterials*, 26 (21) (2005), pp. 4366-4373

[85]P. Li, I. Kangasniemi, K. Groot, T. Kokubo **Bonelike hydroxyapatite induction by a gel-derived titania on a titanium substrate** *J. Am. Ceram. Soc.*, 77 (5) (1994), pp. 1307-1312

[86]G. Schliecker, C. Schmidt, S. Fuchs, T. Kissel **Characterization of a homologous series of D, L-lactic acid oligomers; a mechanistic study on the degradation kinetics in vitro** *Biomaterials*, 24 (21) (2003), pp. 3835-3844

[87]X.-J. Xu, J.C. Sy, V.P. Shastri **Towards developing surface eroding poly (α-hydroxy acids)** *Biomaterials*, 27 (15) (2006), pp. 3021-3030

[88]J.F. Mano, R.A. Sousa, L.F. Boesel, N.M. Neves, R.L. Reis **Bioinert, biodegradable and injectable polymeric matrix composites for hard tissue replacement: state of the art and recent developments** *Compos. Sci. Technol.*, 64 (6) (2004), pp. 789-817

[89]J. Meseguer-Dueñas, J. Más-Estellés, I. Castilla-Cortázar, J.E. Ivirico, A. Vidaurre **Alkaline degradation study of linear and network poly (ε-caprolactone)** *J. Mater. Sci. Mater. Med.*, 22 (1) (2011), pp. 11-18

[90]I. Castilla-Cortázar, J. Más-Estellés, J. Meseguer-Dueñas, J.E. Ivirico, B. Marí, A. Vidaurre **Hydrolytic and enzymatic degradation of a poly (ε-caprolactone) network** *Polym. Degrad. Stab.*, 97 (8) (2012), pp. 1241-1248

[91]A. Vidaurre, J.M.M. Dueñas, J.M. Estellés, I.C. Cortázar **Influence of Enzymatic Degradation on Physical Properties of Poly (ε-caprolactone) Films and Sponges. Macromolecular symposia** *Wiley Online Library* (2008)

[92]Y. Wang, S. Zhang, X. Zeng, L.L. Ma, K.A. Khor, M. Qian **Initial attachment of osteoblastic cells onto sol-gel derived fluoridated hydroxyapatite coatings** *J. Biomed. Mater. Res. A*, 84 (3) (2008), pp. 769-776

[93]S. Jalota, S.B. Bhaduri, A.C. Tas **In vitro testing of calcium phosphate (HA, TCP, and biphasic HA-TCP) whiskers** *J. Biomed. Mater. Res. A*, 78 (3) (2006), pp. 481-490

Materials Science and Engineering: C, Vol. 70, No. 1 (January 1, 2017): pg. 586-598. DOI. This article is © Elsevier and permission has been granted for this version to appear in e-Publications@Marquette. Elsevier does not grant permission for this article to be further copied/distributed or hosted elsewhere without the express permission from Elsevier.